SUPPORTING INFORMATION

Highly Reproducible Hyperthermia Response in Water, Agar and Cellular Environment by Discretely PEGylated Magnetite Nanoparticles.

Idoia Castellanos-Rubio[1,2], Irati Rodrigo[2,3], Ane Olazagoitia-Garmendia[4,5], Oihane Arriortua[1], Izaskun Gil de Muro*[1], José *S. Garitaonandia[6], Jose Ramón Bilbao[4,5,7], M. Luisa Fdez-Gubieda[2], Fernando Plazaola[2], Iñaki Orue[8], Ainara Castellanos-Rubio[4,5,7,9], Maite Insausti[1,3*].*

[1]Departamento de Química Inorgánica, Facultad de Ciencia y Tecnología, UPV/EHU, Barrio Sarriena s/n, 48940, Leioa, Spain.

[2]Departamento de Electricidad y Electrónica, Facultad de Ciencia y Tecnología, UPV/EHU, Barrio Sarriena s/n, 48940, Leioa, Spain.

[3]BC Materials, Basque Center for Materials, Applications and Nanostructures, Barrio Sarriena s/n, 48940, Leioa, Spain.

[4]Departamento de Genética, Antropología Física y Fisiología Animal, Facultad de Medicina y Enfermería, UPV/EHU, Barrio Sarriena s/n, 48940, Leioa, Spain.

[5]Biocruces Bizkaia Health Research Institute, Cruces Plaza, 48903, Barakaldo, Spain.

[6]Departamento de Física Aplicada II, Facultad de Ciencia y Tecnología, UPV/EHU, Barrio Sarriena s/n, 48940, Leioa, Spain.

[7]Spanish Biomedical Research Center in Diabetes and Associated Metabolic Diseases (CIBERDEM), 28029 Madrid, Spain

[8]SGIker, Servicios Generales de Investigación, UPV/EHU, Barrio Sarriena s/n, 48940, Leioa, Spain.

[9] IKERBASQUE Basque Foundation for Science, 48013, Bilbao, Spain.

* Email: (I.C.-R.) idoia.castellanos@ehu.eus

* Email: (M.I.) maite.insausti@ehu.eus

Table of contents

Crystalline size of samples A and B using Scherrer equation

The crystalline sizes of samples A and B have been calculated by the deconvolution of the (311) diffraction peak of magnetite, using the Scherrer equation (S1):

$$D = \frac{K\lambda}{B_{estruc.}\cos\theta} = \qquad \text{(S1)}$$

Where K is the shape factor (0.9-0.95), $B_{structure}$ = $B_{observed}$-$B_{instrumental}$ is the full width at half maximum, λ is the X-ray wavelength (in our case = ($K\alpha_1$+$K\alpha_2$)/2=1.5418Å), and θ is the peak position.

Table S1. Parameters obtained from the deconvolution of (311) of magnetite and crystalline size using Scherrer equation.

Sample	Diffraction peak	B obs. [°2θ]	B inst. [°2θ]	Peak pos. [°2θ]	B struct. [°2θ]	Crystalline size [nm]*
A	311	0.486	0.120	35.598	0.366	23(1)
B	311	0.419	0.12	35,584	0.299	28(1)

**Uncertainty of the calculated sizes is on the last significant digit.*

Hydrodynamic-Size and Zeta-Potential

While sample A@PMAO, coated just by PMAO, has a high Z Potential value, samples with PMAO-PEG have a larger hydrodynamic diameter and a reduced surface charge due to the use of COOH groups in the grafting process of PEG molecules to the PMAO backbone (see **Table S2**). In the case of 23 nm nanoparticles (sample A), the values obtained by the optimized protocol with PEG 5 kDa, PEG 10 kDa and 10 kDa are similar, both in charge and in size. However, for 29 nm nanoparticles (sample B) is necessary a coating with large PEG molecules (PEG 20 kDa) in order to keep the colloid stability. Therefore, only B@PEG20k leads to a successful result.

Table S2. Polydispersity index (PDI), mean hydrodynamic diameter (given in Intensity (Dh_I), Volume (Dh_V) and Number (Dh_N) and Z potential (Pz) for samples A and B with PMAO and PMAO-PEG coatings (PEG 5 kDa, PEG 10 kDa and PEG 20 kDa) using the two different procedures: standard (ST) and optimized (OPT).

SAMPLE	COATING	PDI	D_{hI} (σ)(nm) [H_2O]	D_{hV} (σ)(nm) [H_2O]	D_{hN} (σ)(nm) [H_2O]	Pz (σ) (mV) [H_2O]
A	PMAO	0.20	131(7)	90(9)	54(13)	-37(1.9)
A	PMAO-PEG-10k-ST_	0.13	193(10)	140(3)	111(8)	-2(0.6)
A	PMAO-PEG-5k-OPT	0.20	153(3)	79(9)	55(4)	-12(0.6)
A	PMAO-PEG-10k-OPT	0.19	175(4)	110(4)	78(5)	-8(0.4)
A	PMAO-PEG-20k-OPT	0.19	166(9)	104(2)	74(1)	-7(0.6)
B	PMAO-PEG-5k-OPT	0.65	476(7)	466(7)	68(2)	-31(0.6)
B	PMAO-PEG-10k-OPT	0.46	548(53)	134(38)	82(10)	-27(0.2)
B	PMAO-PEG-20k-OPT	0.30	280(7)	158(9)	81(1)	-8(0.6)

Refinement of the PMAO-PEG coating protocol.

In order to attain individually or quasi-individually coated FM-NP formulations, an optimization of the coating protocol was carried out. **Table S3** and **Figure S1** summarize representative sample A@PEG10k preparations, in which one coating parameter at a time was modified. The agglomeration degree of the FMNPs in these preparations can be deduced from the dynamical hysteresis loops shape and the corresponding SAR vs H curves. The effect that the coating conditions (**Table S3**) have on the SAR are visible in the **Figure S1**.

Table S3. Summary of the parameters used in the coating procedure of some representative preparations: PMAO monomers added per nm^2 of NP surface, concentration of the PMAO-PEG copolymer, solvent of the PMAO-PEG stock solution, strategy used to mix the FM-NPs with the PMAO-PEG and the corresponding SAR value obtained in the final A@PEG aqueous colloid.

Preparation	Monomers/nm^2	[PMAO-PEG] (mg_{PMAO}/ml)	Solvent of the PMAO-PEG stock	Mixing Strategy (FMNPs + PMAO-PEG)	SAR (W/g) at 38 mT and 300 kHz
1	100	0.5	$CHCl_3$	pouring	280
2	50	0.5	$CHCl_3$	pouring	490
3	25	0.5	$CHCl_3$	pouring	270
4	50	0.5	$CHCl_3$:EtOH *	pouring	405
5	50	0.5	$CHCl_3$:Hexane *	pouring	365
6	50	0.5	$CHCl_3$	dropwise	570
7	**50**	**5**	**$CHCl_3$**	**dropwise**	**670**

* The solvent mixture is in 1:1 relation

Preparation 1

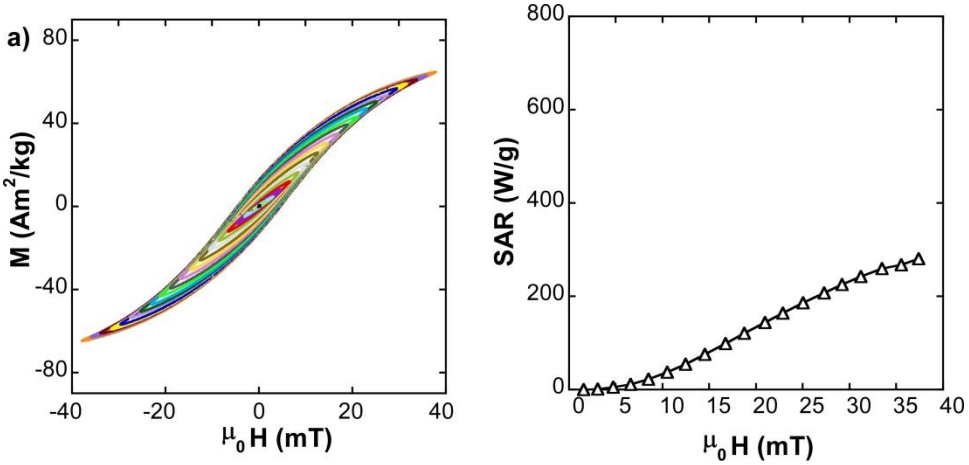

Preparation 2

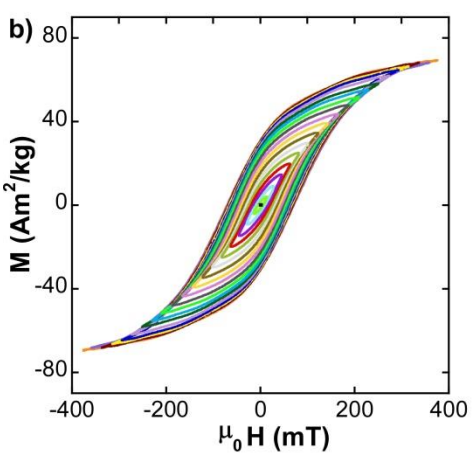

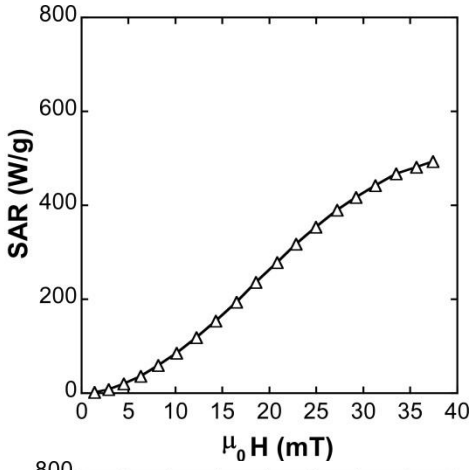

Preparation 3

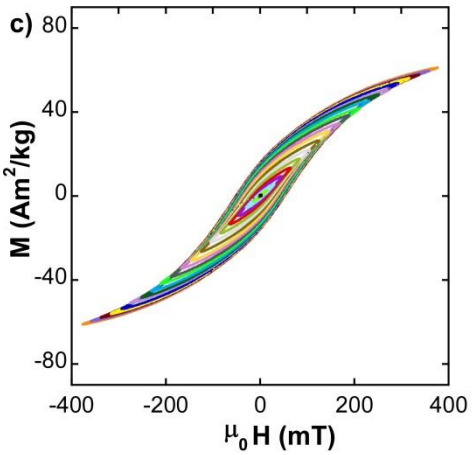

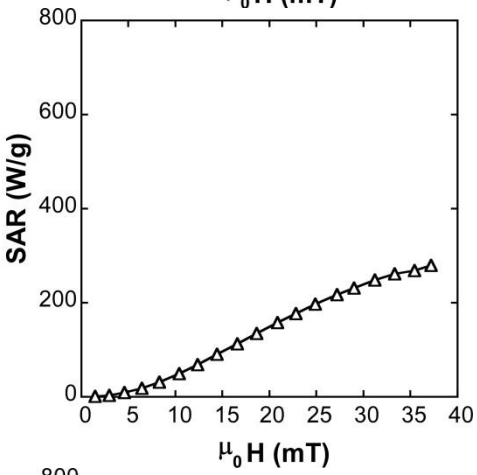

Preparation 4

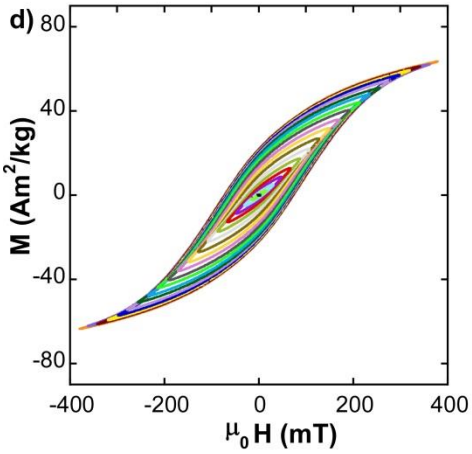

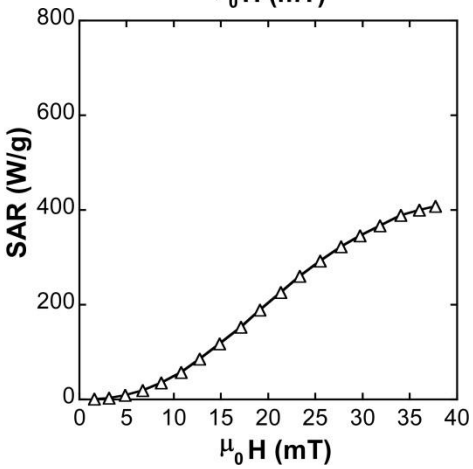

Preparation 5

Preparation 6

Preparation 7

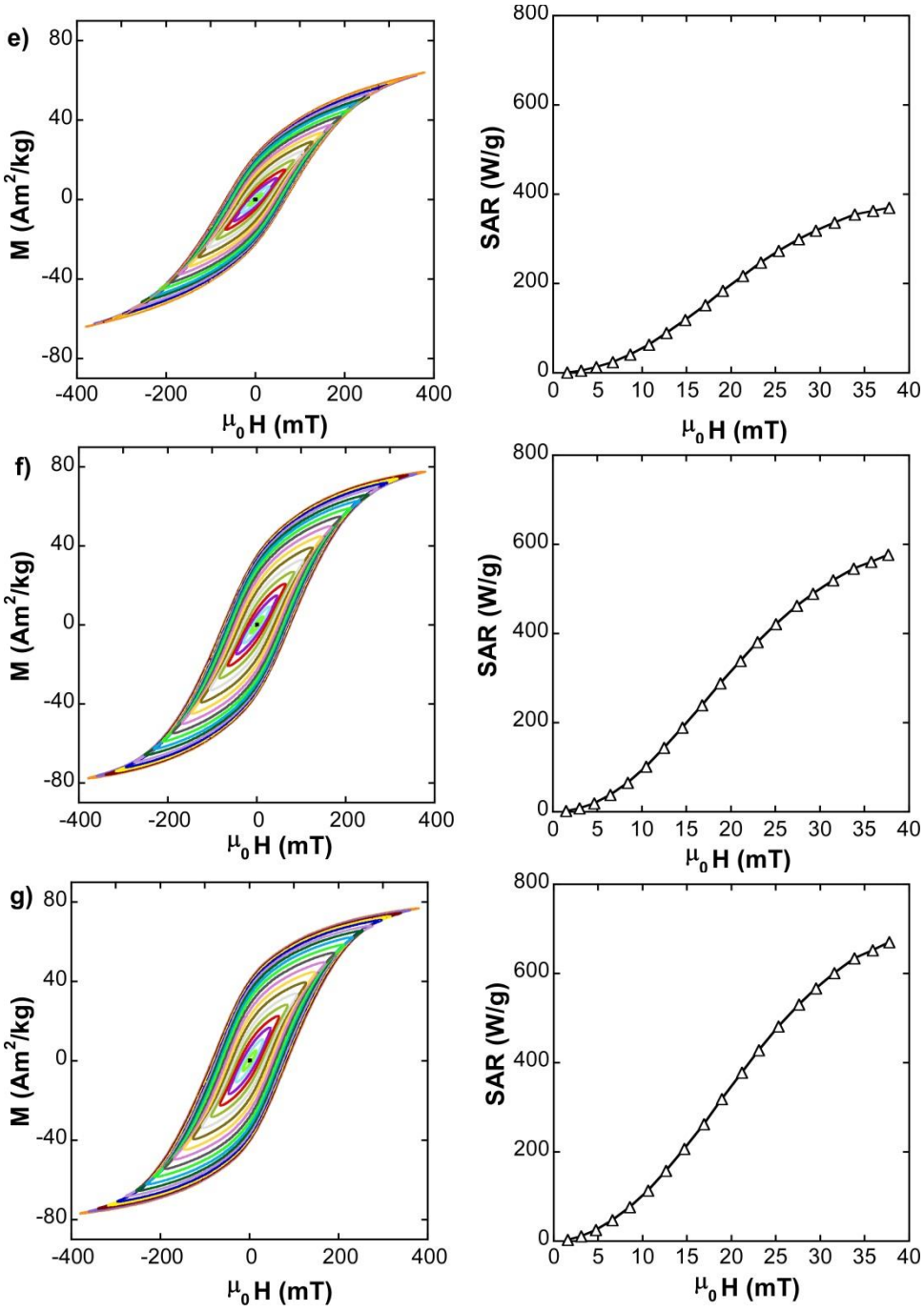

Figure S1. AC hysteresis loops and the corresponding experimental SAR vs field curves of representative sampleA@PEG preparations. Preparations 1-7: a)-g)

Analysis over the coating thickness

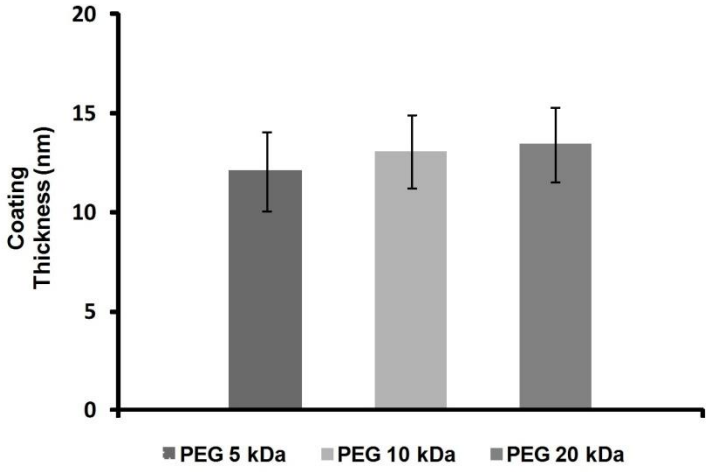

Figure S2. Analysis of the PMAO-PEG copolymer thickness in sampleA@PEG with PEG 5 kDa, PEG 10 kDa and PEG 20 kDa .

The bar plot of **Figure S3** compares the coating thickness of the three PMAO-PEG copolymers used (PEG= 5 kDa, 10 kDa and 20 kDa). The mean value and standard deviation in each case have been obtained from the negative staining TEM micrographs. The determine polymeric thickness of sampleA@PEG (5,10 and 20 kDa) turned out to be analogous. Taking into account that the percentage of PEG molecules grafted into the PMAO backbone is the same in the three cases (75% of the total monomers), this effect seems to be due to a greater folding of longer PEG chains around the particles. Thus, it can be concluded that PMAO-PEG20k coating presents higher density than PMAO-PEG with 5 and 10 kDa.

Model S1: Theoretical Modeling of colloidal stability

The interaction energy between two Fe_3O_4 NPs coated by PEG in an aqueous suspension has been calculated using a modified DLVO model, as presented by O. T. Mefford el. al. [*Chem. Mater.*, **2008,** 20, 2184]. In this model, the potential energy (V_{total}), resulting from the superposition of attractive and repulsive forces, is given by the Equation S2:

$$V_{total} = V_{vdW} + V_{mag} + V_{ES} + V_{Steric} \quad (S2)$$

where V_{vdW} comes from the van der Waals attractive forces, V_{mag} is the attractive magnetic dipolar interaction energy between point magnetic dipoles, V_{ES} is the electrostatic repulsive potential energy between charges of the same sign and V_{Steric} is the steric repulsive potential energy.

In the present case, van der Waals interaction takes the following form:

$$V_{vdW} = -\frac{1}{6} A_{eff} \left(\frac{2r_c^2}{r^2 - 4r_c^2} + \frac{2r_c^2}{r^2} + \ln\left(\frac{r^2 - 4r_c^2}{r^2} \right) \right) \quad (S3)$$

where A_{eff} is the so-called retarded Hamaker constant ($5.47 \times 10^{-19}\, J$), r_c is the magnetic nanoparticle (core) radius and r is the center to center distance of the two colloidal particles.

The magnetic dipolar energy cannot be expressed, in principle, as a simple function of inter-particle distance (it is not a central potential energy) as can be done for the rest of terms in Equation (S7). This interaction is essentially anisotropic because depends on the relative orientation of the two particle dipoles. Given that here we are making an estimation of the total energy (V_{total}), for simplicity one can use the following "central" approximation for the magnetic dipolar energy:

$$V_{mag} \approx -\frac{4\pi\mu_0 r_c^6 M^2}{9r^3} \quad (S4)$$

where M is the particle Magnetization.

The electrostatic potential energy is the corresponding one to two identical spheres of radius r_h (radius of the colloidal particle or hydrodynamic radius) located at a distance of r:

$$V_{ES} \approx \frac{4\pi\varepsilon_0 r_h^2 V_z^2}{r} \qquad (S5)$$

where V_z is the surface charge or Zeta potential. Since the Zeta potential of our FM-NPs@PEG systems is low (see **Table S2**) and in physiological solutions the salt ions screen the surface charges of the particles, the electrostatic repulsion can be neglected.

The last term in Equation (S2) (V_{Steric}) corresponds to the steric repulsion, which according to that proposed by C. N. Likos et. al. [*Phys. Rev. Lett.*, **1998**, *80* (20), 4450] is given by:

$$V_{steric} = \frac{5}{18} k_B T f^{3/2} \begin{cases} -\ln(r/\sigma) + \left(1 + \sqrt{f}/2\right)^{-1} & r \leq \sigma \\ \left(1 + \sqrt{f}/2\right)^{-1} (r/\sigma) \exp\left(-\sqrt{f}\,(r-\sigma)/2\sigma\right) & r > \sigma \end{cases} \qquad (S6)$$

where f is the number of polymeric chains per particle and σ is 1.3 times the radius of gyration (R_g). Since the colloidal particles are compose of pseudo-spherical magnetite core and polymeric spherical shell, the radius of gyration of this core-shell structure is given by Equation S7:

$$R_g = \left(\frac{I_{c-s}}{M_c + M_s}\right)^{1/2} = \left\{\left(\frac{1}{M_c + M_s}\right)\left(\frac{2}{5} M_c r_c^2 + \frac{2}{5} M_s \left[\frac{r_h^5 - r_c^5}{r_h^3 - r_c^3}\right]\right)\right\}^{1/2} \qquad (S7)$$

where M_c and M_s are the mass of the core and shell respectively. The mass of the core M_c is simply the density of magnetite ($5200\ kg/m^3$) times the particle volume ($M_c = \rho_{Fe3O4} \times (4/3)\pi r_c^3$), and the mass of the shell M_s is the number of polymeric chains per particle (f) multiplied by the molecular weight of each molecule ($1kDa = 1.66 \times 10^{-24}\ kg$). Note that once the number of

PEG molecules per surface unit of the core surface ($\#PEG/nm^2$) is known, the number of polymeric chains f is given by: $f = \#PEG/nm^2 \times 4\pi r_c^2$.

The parameters and values used for the calculation of V_{total} in samples A@PEG and B@PEG are summarized in **Table S4** and detailed below:

- Diameter of the inorganic core (D_c):

  These values have been taken from TEM measurements (Table 1 in the manuscript).

  Therefore, r_c from Equations S8, S9 and S12 is: $r_c = \frac{D_c}{2}$

- Magnetic moment of the FM-NPs (M)

  The saturation magnetization of the samples at RT has been used (Table 1 in the manuscript).

- Hydrodinamic diameter (D_h)

  The negative staining analysis of the three polymeric coatings (5, 10 and 20kDa) in TEM displays similar thickness. However, this thickness value cannot be used as D_h because it corresponds to dry samples where the polymeric shells most likely have got shrunk. Data from DLS analysis also show similar sizes for the three PEG coatings. In order to employ values closer to individual coatings and avoid overestimation of larger aggregates **D_{hN}** (**Table S2)** parameter has been chosen for the calculations. Thus, $r_h = \frac{D_h}{2}$ in Equations S5 and S7.

- PEG amount per surface unit (#PEG/nm^2)

  TG measurements (**Figure S8**) of Sample A and B, prior to coating, give rise to 3-5 oleic acid (OA) molecules per nm^2 of NP surface, which is in agreement with previous results [I. Castellanos-Rubio et. al., *Nanoscale* **2014**, *12*, 7542]. Since it is expected 0.75 PEG molecules to be incorporated for each OA on the surface (*OA:PMAOmonomer ratio* on the NP should be *1:1* [J. L. Chen et. al., *Small* **2008**, *4* (3), 334] and 75% of PMAO monomers are grafted with PEG, see *Experimental Section),* between 2-4 PEG molecules per nm^2 are estimated.

2 PEG /nm^2 have been used for the calculation based on previous experimental data [S. Saville et. al., *Nanoscale* **2013**, *5* (5), 2152].

- Density of the inorganic core and of the polymeric shell (ρ_{core}, ρ_{shell})

$$\rho_{core} = density\ of\ Fe_3O_4 = 5200\ kg/m^3$$

$$\rho_{shell} = \frac{2PEG/nm^2 \times 4\pi r_c^2 \times M_{wPEG}}{(4\pi r_h^3 - 4\pi r_c^3)}$$

Table S4. Summary of the parameters and values used in the calculation of V_{Total} for samples A@PEG and B@PEG. Diameter of the inorganic core (D_{core}), Magnetic moment of the inorganic core (M), Molecular Weight of the PEG (Mw_{PEG}), Hidrodynamic diameter (D_h), Radius of gyration (R_g), Number of PEG molecules per nm^2 of NP surface (#PEG/nm^2), Density of the inorganic core (ρ_{core}), Density of the polymeric shell (ρ_{shell}), Equilibrium distance (r_e) and Energy barrier of the potential well (ΔE).

Sample	D_c (nm)	M (Am^2/kg)	Mw_{PEG} (kDa)	D_h (nm)	R_g (nm)	#PEG /nm^2	ρ_{core} (kg/m^3)	ρ_{shell} (kg/m^3)	r_e (nm)	ΔE (ev)	ΔE (K_BT)
A@PEG5k	23	85	5	74	16.9	2	5200	134.1	27.1	0.4	14
A@PEG10k	23	85	10	74	19.3	2	5200	268.1	32.3	0.2	6
A@PEG20k	23	85	20	74	21.1	2	5200	536.2	35.8	0.1	3
B@PEG5k*	29	90	5	81	17.96	2	5200	165.2	--	--	--
B@PEG10k*	29	90	10	81	20.6	2	5200	330.4	--	--	--
B@PEG20k	29	90	20	81	22.8	2	5200	660.8	35.9	0.5	19

** There is no potential well, V_{Total} is almost purely attractive for samples B@PEG (5 and 10 kDa)*

Figure S3 shows the results of applying the DLVO model (described by the Equations S2-S7) to samples A@PEG and B@PEG. Specifically, **Figure S3-a** displays the estimated potential energy as a function of center to center distance of A (23 nm) particles coated with different PEGs (5, 10 and 20 kDa), the three cases present asymmetrical potential wells with moderate depth ($\Delta E < 0.5$ eV). The minima of potential energy become less deep and shifted towards larger center-center distances when the Mw of the PEG is higher, meaning a better long-term colloidal stability. Experimentally it was observed that sample A formed stable colloids in the short to medium term (≤96 h, confirmed during cytotoxicity assay) and presented similar hydrodynamic diameter and heating efficiencies with the three PEGs.

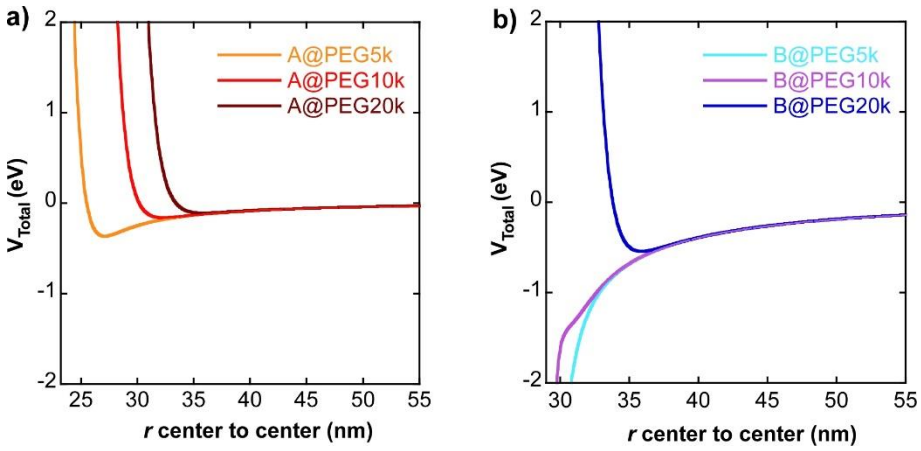

Figure S3. Particle to particle potential energy as a function of center to center distance using DLVO model for **a)** Sample A@PEG (5, 10 and 20 kDa) and **b)** Sample B@PEG (5, 10 and 20 kDa. The data for the calculation have been taken from **Table S4.**

However, the colloidal stability of sample B (29 nm) dramatically decreased when the Mw of the PEG used in the coating was lower than 20 kDa, so B@PEG (5 and 10 kDa) gave rise to larger aggregates (see D_h in **Table S2)** and lower SAR values. **Figure S3-b** illustrates the critical transformation of the potential curve when the polymeric coating of sample B is formed by 20 kDa PEG. In fact, B@PEG (5 and 10 kDa) systems produce almost purely attractive potential energies where the steric contribution is negligible; and on the contrary, the potential energy becomes basically repulsive for B@PEG20k system with an equilibrium distance and a well depth comparable to A@PEG5k system (see **Table S4**). Thus, the numerical output extracted from this model supports that the increase of the polymeric shell density in the case of PEG-20kDa is able to enlarge the steric repulsion of B particles enough to confer them satisfactory colloidal stability.

In addition, these calculations can be extended to different MNPs to predict suitable PEG coatings. As the density of PEG (1-10 kDa) in aqueous solution is around 1050 (kg/m^3) at RT [P. González-Tello et. al., *J. Chem. Eng. Data* **1994**, *39* (3), 611], it seems fair to keep ρ_{shell} below that value. **Table S5** and **Figure S4** show some examples of Fe_3O_4 NPs of 35 nm coated with PEGs of

different molecular weight. It can be inferred from the V_{Total} calculation that this NP system would need a PEG of 30 or 40 kDa (keeping ρ_{shell} at a reasonable value) to reach enough colloidal stability.

Table S5. Summary of the parameters and values used in the calculation of V_{Total} for Fe_3O_4 NPs of 35 nm with PEG coating of 20, 30 and 40 kDa. Diameter of the inorganic core (D_{core}), Magnetic moment of the inorganic core (M), Molecular Weight of the PEG (Mw_{PEG}), Hidrodynamic diameter (D_h), Radius of gyration (R_g), Number of PEG molecules per nm^2 of NP surface (#PEG/nm^2), Density of the inorganic core (ρ_{core}), Density of the polymeric shell (ρ_{shell}), Equilibrium distance (r_e) and Energy barrier of the potential well (ΔE).

Example	D_{core} (nm)	M (Am^2/kg)	Mw_{PEG} (kDa)	D_h (nm)	R_g (nm)	#PEG /nm^2	ρ_{core} (kg/m^3)	ρ_{shell} (kg/m^3)	r_e (nm)	ΔE (ev)	ΔE (K_BT)
X@PEG20k	35	90	20	92	25.5	2	5200	660.8	37.8	1.6	62
X@PEG30k	35	90	30	92	26.7	2	5200	**990.8**	40.5	1.1	42
X@PEG30k	35	90	30	105	30.0	2	5200	660.8	46.4	0.6	24
X@PEG40k	35	90	40	115	33.6	2	5200	660.8	52.5	0.4	15

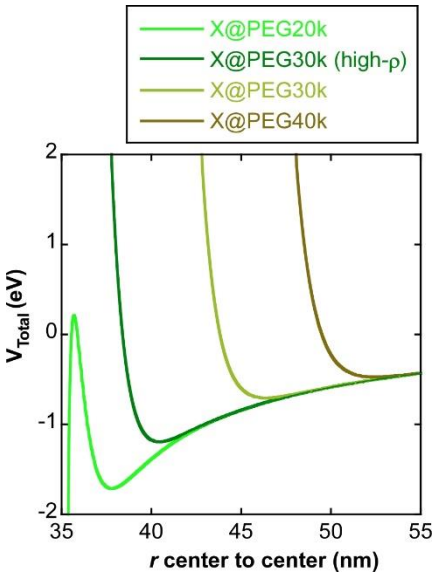

Figure S4. Particle to particle potential energy as a function of center to center distance using DLVO model for Fe_3O_4 nanoparticles of 35 nm in diameter coated by PEGs of different molecular weight. The data for the calculation have been taken from **Table S5**.

To sum up, this semi-quantitative model allows for a better understanding on how the density of the polymeric coating affects the steric repulsive force, providing a plausible explanation for the different colloidal stabilities produced by polymeric coatings of similar thicknesses.

AC loops of optimized A sample@PEG (5kDa and 10kDa) in Agar and physiological media

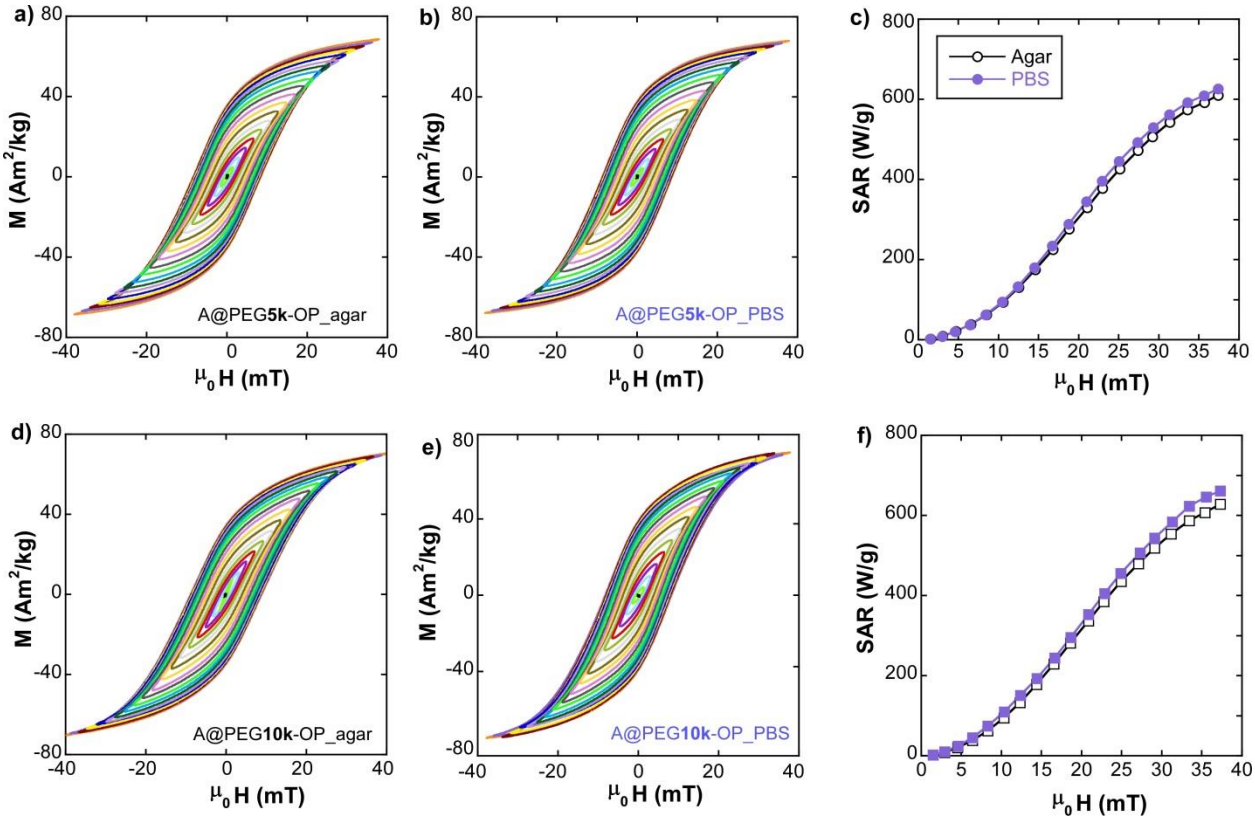

Figure S5. AC hysteresis loops (a,b,d,e) and the corresponding experimental SAR vs field curves (c,f) of sampleA@PEG5k-OP and sampleA@PEG10k-OP on Agar and PBS.

Model S2: Hysteresis loops simulation of DC and AC loops.

The high energy barrier approach, as followed in this work, is a Stoner-Wohlfarth based model (SWBM). In this, magnetization is able to take only discrete orientations because it is assumed that thermal energy $k_B T$, is much smaller than the anisotropy energy $K_{eff} v$, where K_{eff} the anisotropy energy density and v, the particle volume. The dynamical problem is therefore reduced to the calculation of the probabilities $p_i(t)$ of finding the magnetization in any of the minimum energy states *i* at a given time *t*, as determined from the energy landscape of the system, $E(\theta, \varphi, t)$. This method was developed explicitly by Carrey et al (*J. Carrey, B. Mehhaoui and M. Respuad, J. Appl. Phys, 109 083921 (2011)*) for the case of uniaxial single domain magnetic particles, where magnetization depends only on the polar angle (a one dimensional problem). The approach can be generalized for more complex 2-dimensional problems (magnetization depending on both polar and azimuthal angles), as those involving the cubic, mixed or multiaxial anisotropies (*C. J. Geoghegan, W. T. Coffey and B. Mulligan, Advances in Chemical Physics, Vol 100, Ed: I. Prigogine and S. A. Rice, Wiley&Sons, 1997*).

The instantaneous magnetization of each particle is given by:

$$M_H(t) = M \sum_i p_i(t) \hat{u}_i(t) \cdot \hat{u}_H(t) \qquad \text{(S8)}$$

In equation (S2) the unit vectors $\hat{u}_i(t)$ define the directions of the minima states that, in general, depend on the sinusoidal magnetic field given by $H(t) = H_0 sin\omega t\, \hat{u}_H$, being $f = 2\pi/\omega$ the frequency of AC field and $\hat{u}_H$ the magnetic field unit vector. The time evolution of the probabilities $p_i(t)$ can be calculated by solving a set of ordinary differential equations as:

$$\frac{\partial p_i}{\partial t} = \sum_{j \neq i} w_{ji} p_j - \left(\sum_{j \neq i} w_{ij} \right) p_i \qquad \text{(S9)}$$

where index i runs through the total number of minima. This equation is a way of saying that the change of the population in minimum i is the result of all the incoming jumps (first term) from the available neighbor states minus those departing from i (second term), with the condition $\sum p_i = 1$, which states that magnetization M is constant. The coefficients w_{ij} denote the rate of jumps (in units of frequency) from state i to state j, which depend on the instantaneous energy barrier E_{ij}, as $w_{ij}(t) = c_{ij}\exp(-vE_{ij}/k_BT)$, being v the volume of the single domain and pre-factor c_{ij} being the maximum jumps rate related to the natural precession frequency of the particle magnetization, which has been considered a constant equal to 10^{-10} s.

The case of an effective uniaxial anisotropy.

If dipolar interactions can be neglected, the energy landscape of the magnetic single domain is in general function of two space variables, for instance the polar θ and azimuthal φ angles of spherical coordinates, and the time t (or the external magnetic field which in turn is a function of time): $E(\theta, \varphi, t)$. For uniaxial magnetic anisotropy, the energy landscape does not depend on the azimuthal angle and therefore becomes a function of θ and t:

$$E(\theta, t) = K_u sin^2\theta - \mu_0 M H_0 sin\omega t cos(\theta - \phi) \qquad (S10)$$

where θ is the angle between the single domain magnetic moment and the magnetic easy axis and ϕ is the angle between the external magnetic vector field and the easy axis. In these conditions the energy has two minima in general and equation (S9) reduces to:

$$\frac{\partial p_{1(2)}}{\partial t} = w_{21(12)} p_{2(1)} - w_{12(21)} p_{1(2)} \qquad (S11)$$

When the easy axis is oriented at random respect to the external applied field, the magnetization should be averaged over all the possible orientations between the easy axes and the external magnetic field ϕ, as:

$$M_{random} = \frac{\int_{\phi=0}^{\phi=\pi/2} M_H(t) sin\phi d\phi}{\int sin\phi d\phi d\phi} \qquad (S12)$$

DC hysteresis loops, as those obtained in a SQUID magnetometer at 5 K, can be simulated in this framework by using a low frequency excitation (1 Hz), while AC loops can be obviously calculated following the experimental frequencies of hyperthermia.

Effective anisotropy constant distribution

The existence of distributions of sizes and/or shapes/morphologies is inherent to real nanoparticles fabrication. At best, given a certain synthesis protocol, morphology is broadly determined (for instance, strongly faceted cube-octahedral) but fine details of individual particles reveal the onset of different elongations, face extrusions or irregularities in general as well as certain distribution of sizes. All these features introduce uncertainties that must affect significantly important properties as the magnetic anisotropy constant or the rate of jumps between energy minima in $w_{ij}(t)$. At very low temperatures, the influence of size dispersity is expected to be negligible (ratio $vE_{ij}/k_B T$ is very large in any case) so the influence of anisotropy constant dispersion should be dominant. For this reason, simulations performed according to the previously described model have been obtained by averaging loops over a normal distribution of anisotropy constants, even the AC loops calculated at room temperature. However, it should be kept in mind that size distribution

and even dipolar inter-particle interactions should play a role that has been implicitly included in the anisotropy distribution. Probably, the large dispersion of anisotropies needed to fit the experimental AC loops at room temperature (around 5 kJ/m^3, relative to an average of $\langle K_u \rangle$ =13.5 kJ/m^3) reflects in fact the underlying impact of these additional effects.

Figure S6 shows the hysteresis loops calculated for sample A and B at a frequency of 300 kHz with increasing external field amplitude. Each loop, as shown in **Figure S6**, results from averaging around 800 single simulations, each one corresponding to an angle ϕ and anisotropy constant K_u.

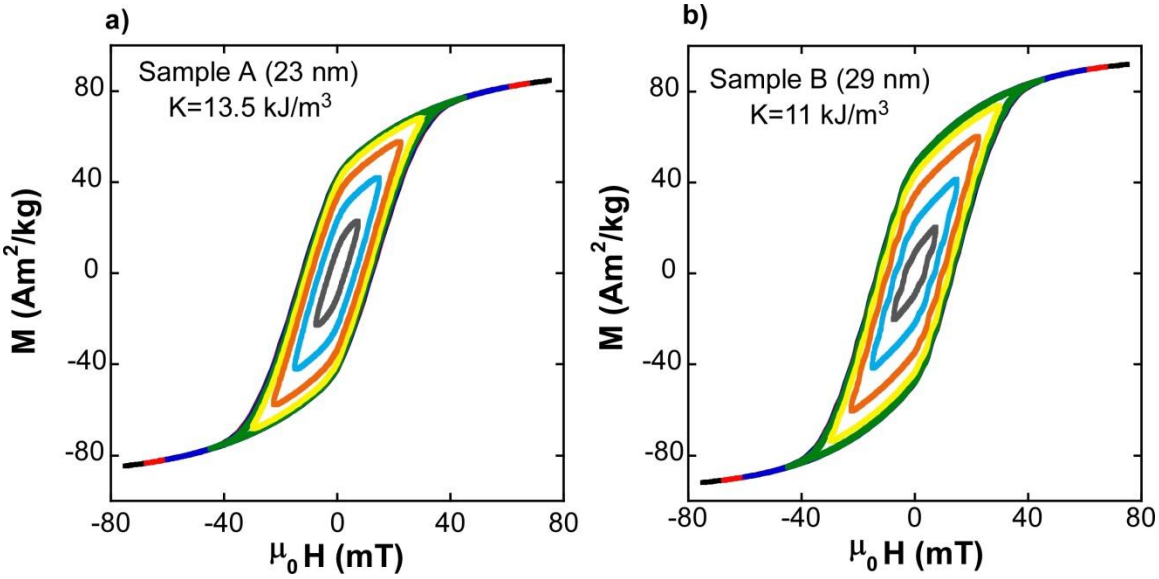

Figure S6. (a) Calculated hysteresis loops under an AC excitation at 300 KHz for sample A with an average anisotropy constant of 13.5 kJ/m^3.**(b)** Calculated hysteresis loops calculated under an AC excitation at 300 KHz for sample B with an average anisotropy constant of 11 kJ/m^3.

Frequency dependency of SAR in sample A.

The higher or lower influence of the excitation frequency on the hysteresis Area is expected to depend on the particle size. This influence takes place through thermal fluctuations, in other words, due to the different ratio of the thermal energy $k_B T$ to the anisotropy energy $K_{eff} v$. Stoner-Wohlfarth-Based Models are able to predict that particles of 23 nm display this feature, as observed in **Figure S7**. Simulations performed under the same parameters but at different frequencies fit well to the experimental observation.

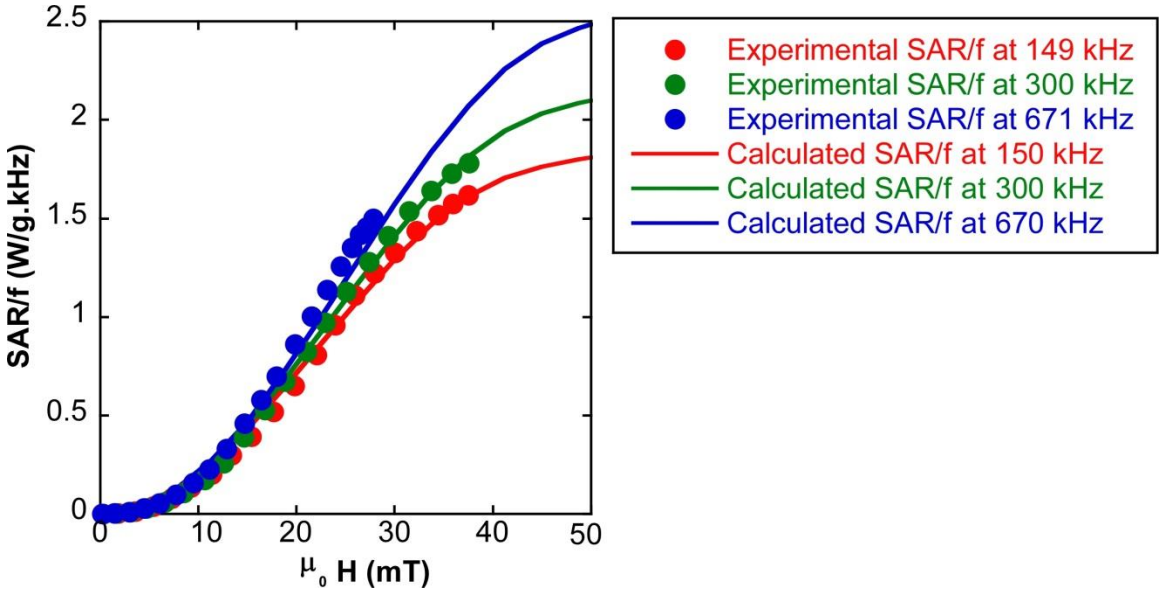

Figure S7. Solid circles correspond to experimental SAR obtained at 670 kHz (blue colored), 200 kHz (green colored) and 150 kHz (red colored). Solid lines correspond to the calculated SAR versus H curve obtained from simulations by taking $= 13.5\ \mathrm{kJ/m^3}$, standard deviation of K distribution of $5\ \mathrm{kJ/m^3}$ and magnetization $\mathrm{M} = 85\ \mathrm{Am^2/kg}$.

Thermogravimetric measurements

The thermogravimetric measurements of samples A and B prior to the polymeric coating are displayed in **Figure S8**. The organic matter percentage determined by thermogravimetry is 8.1 % and 5.7 % respectively, which corresponds to ≈ 4 oleic acid molecules per nm^2 of FM-NP surface.

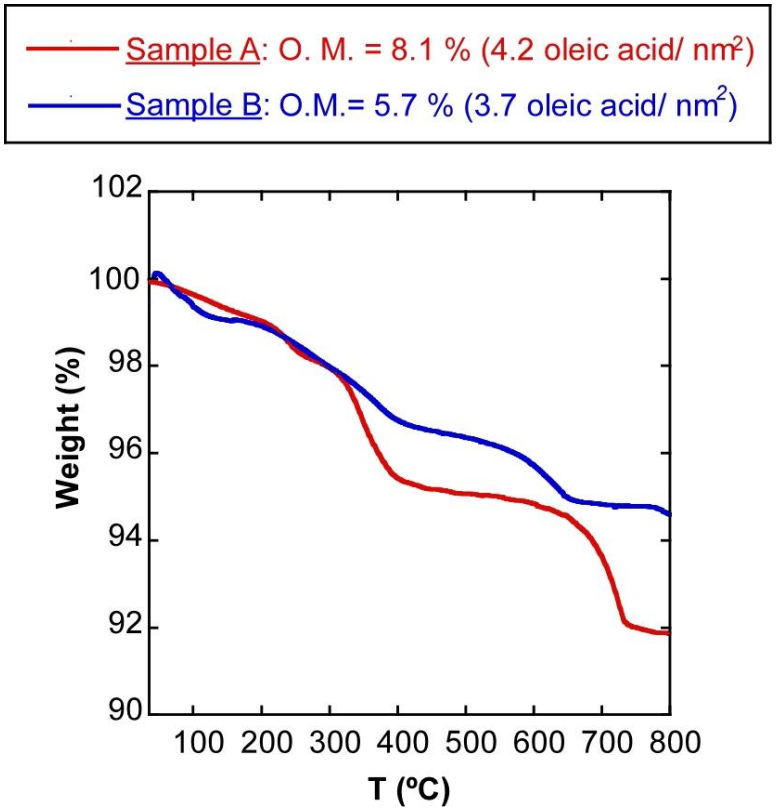

Figure S8. Thermogravimetric measurement of samples A and B prior to polymeric coating.